The Cooling Design of a High-Speed Rotating Axis with Ribbed Turbulators

Sheng-Chung Tzeng*, Tzer-Ming Jeng , Yen-Chan Wang

Department of Mechanical Engineering, Chienkuo Technology University, Taiwan, ROC

Abstract

This work experimentally and numerically investigated the heat transfer characteristics of the high-speed rotating axis of five-axis processing machines. The test section of rotation axis possesses the novel design with ribbed turbulators to strengthen heat dissipation. A good cooling design will reduce the coefficient of thermal expansion, the thermal deformation and the damage of cutting tools to enhance the delicacy and the efficiency of the processing machining. In order to make the analysis meaningful, the experimental condition was made as close to the working of the real high-speed rotation axis as possible, and the oil was employed as the coolant. The relevant experiments analyzed the heat transfer distributions in radial directions and the axial directions of the rotor located in the test section of round cylinder with different rotational speeds. The empirical formula based on the test results was proposed to provide critical references for machining delicacy improvement in five-axis processing machines.

Keywords: heat transfer, high-speed rotation, five-axis processing machine, ribbed turbulators

1. Introduction

The technical research and development of modern machine tools advance at a tremendous pace. The demand of machine tools has changed from traditional lathes and milling machines to tool machines for special purposes, such as high-speed five-axis processing machines. To meet the growing demand, the following development of various kinds of high-speed five-axis processing machines is growing mature. Nowadays, the drive of the main shaft of a regular high-speed five-axis processing machine is about 6~9kW and its rotational speed of the main shaft is about 5,000~50,000rpm. Since the workpiece of high-speed five-axis processing machines is a complicated 3D district, the accurate degree in processing is relatively high as well. A regular work piece of complicated geometry needs to relay on a high speed of five-axis processing machines. As for increasing the accuracy, the key factors are to decrease the damage of cutting tools and to improve the cooling and lubricating of high-speed rotational shafts.

Researches in the rotating axis of the general fluid recently, Song et al. [1] experimentally measure the heat transfer performance of axial rotating heat pipes at rotational speeds up to 4000rpm. A cylindrical and an internally tapered heat pipe with water as the working fluid were tested with different fluid loadings that ranged from 5% to 30% of the total interior volume. Bouafia et al [2] proposed the experimental results of convective heat transfer in an annular gap flow, between a heated rotating inner cylinder and a cooled stationary outer cylinder with or without axial flow. This study results for rotational flow without

──────────────────────

∗ Corresponding author. E-mail address: tsc@ctu.edu.tw

Tel.: 886-4-7111111 ext 3192; Fax: 886-4-7357193

axial flow reveal the interest of the presence of grooves and an important heat transfer as the velocity increase. In presence of axial flow, their investigations conducted in turbulent flow show that the situation of a smooth air gap is more favorable for heat transfer at the rotor. Hwang and Lai [3] indicated the three-dimensional mixed convection for a constant-property laminar fluid flow through a periodical two-pass square channel with radial rotation is presented. Kolyshkin and Vaillancourt [4] studied linear stability of Couette flow with rotating inner cylinder and radially nonuniform internal heat sources. Yan and Soong [5] developed mixed convection in radially rotating rectangular ducts. Soong and Yan [6] investigated the development of secondary flow and convective heat transfer in isothermal/iso-flux rectangular ducts rotating about a parallel axis. Soong et al. [7] presented the experimental work on the qualitative nature of three-dimensional flow structure between two rotating co-axial disks at a relatively wide range of rotational conditions. They revealed distinct flow structure between two disks rotating at various conditions and provided profound insights for better understanding of fundamental mechanisms of the complex three-dimensional rotating flows that are valuable in analysis and design of rotating flow systems.

This study is mainly discussing about the coefficient of the high-speed rotation axis of five-axis processing machines, and will focus on researches about rotating axis with ribbed turbulators to provide design reference for high-speed rotating spindles. The experiment is targeted at the actual geometric dimension and operating parameter of the rotating axis of the five-axis machine and taking the relevant physical parameters of the most advanced high-speed five-axis machining tool as references. The current design of rotating axis can lead to high temperature in some regions, and this may cause the delicacy of machining not good enough. If the contact area of heat convection of cooling lubricant could be increased, adding the spoiler ribs can improve the unevenness of temperature distribution and the thermal expansion produced in rotating high-speed axis. The limitation of high flow resistance can also be overcome and the efficiency of heat convection can be increased dramatically. This technology can reduce the coefficient of thermal expansion and improve the delicacy of machining. Those improvements will bring significant economic benefits for the precision processing industry. For instance, the yield of processing can be better, the cost of processing can be lower, and the operating time of this kind of advanced machining equipment can be longer.

2. Experiments and Methodology

2.1. Experimental Equipments and Test Section

All experimental equipment, shown in Fig. 1, can be divided into five parts: experimental test section, thermocouples, rotating spindle, oil cooling system, and data acquisition system. Descriptions for the main experimental devices are as followed: the experimental test section is made up of the smooth wall and four different ribbed walls. There were 19 temperature measurement points placed in the inner wall shell of the experimental test section. The main power source of the experimental rotating spindle is high-speed AC motor and it also equipped with an inverter to control the rotational speed to simulate the practical rotation of axis.

The various rotational speeds in this experiment are 0, 500, 750, 1000, 1250, 1500, 1750, 2000, 2250, and 2500. The cooling oil is used as the high quality cooling lubricant. The oil cooling system uses two sets of storage tanks. One is for forcing the cooling oil to be transported to the interior of the test section and there are four kinds of flow rates: $2.083 \, cm^3/s$, $5.279 \, cm^3/s$, $6.994 \, cm^3/s$, and $9.635 \, cm^3/s$. The other is for oil returning. The temperature measurement of the test section is to measure the signals of measure points by TT-T-30SLE high precision thermocouples. Measured signals will be transferred to reading data of temperature.

1. Oil tanks
2. Test section
3. Data recorder
4. Personal computer
5. Power slip ring
6. Tachometer
7. Power supply
8. Motor
9. Inverter
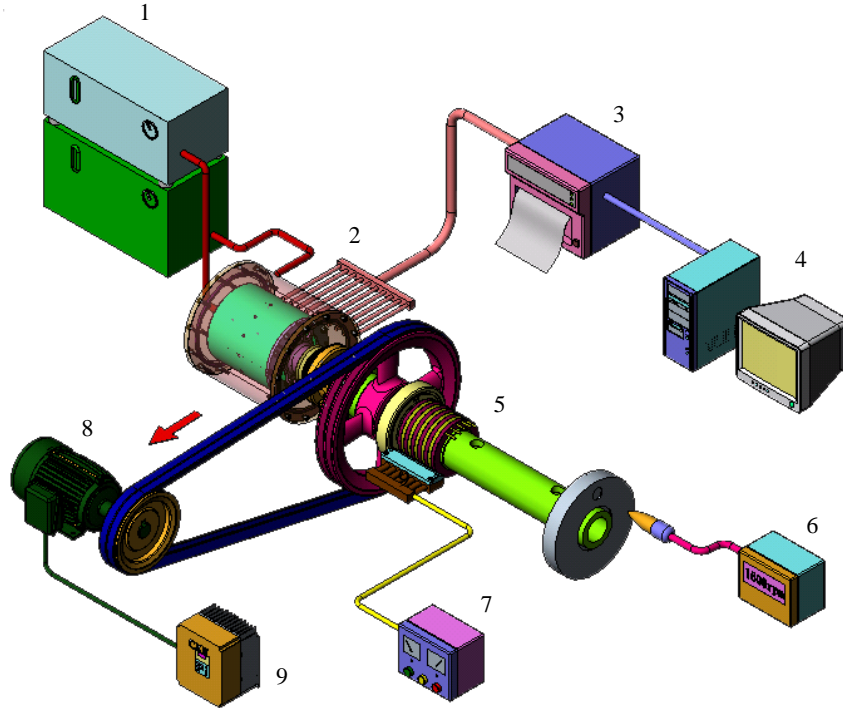
Fig. 1 Experimental apparatus
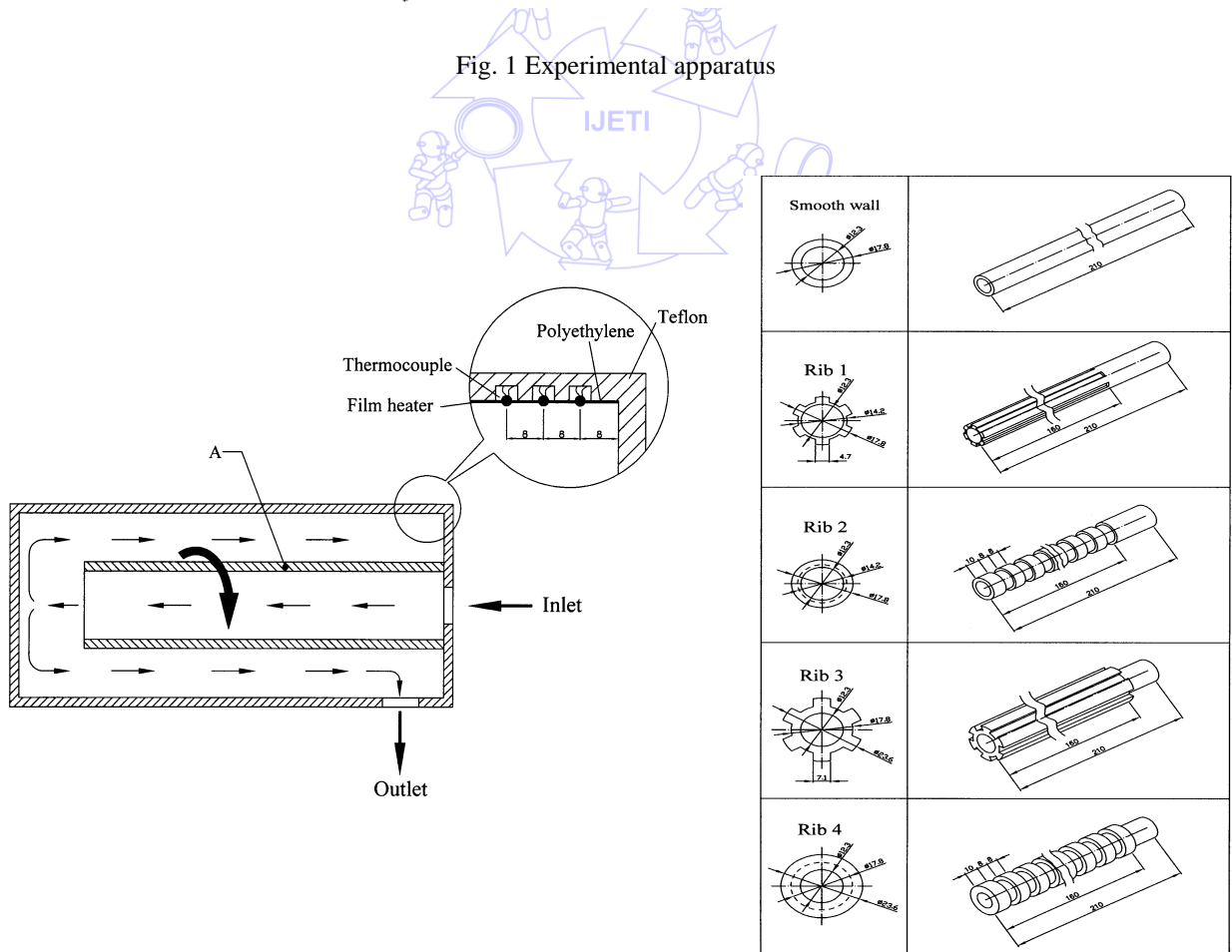
Fig. 2 Configurations of test sections

The test section can be divided into the internal rotating axis and the external stationary cylinder. The basic material for the external cylinder is Telfon and to heat by a DC power supply and power slip ring. The heating area is a 0.012m^2 stainless steel of high resistance heating film (the resistance is 30.7ohms) using the glue with excellent thermal conductivity as adhesives to fix the heating film on the heating section. To respectively measure the local heat transfer distribution in axial and side wall, nineteen measure points were buried evenly in the axial direction to output the temperature data. The diameter of the internal rotating cylinder is 0.0174m. The diameter of the external stationary cylinder is 0.05m. Test section is shown in Fig. 2 in this study.

2.2. Data Reduction

All the measured data could be reduced to be the following relevant dimensionless parameters.

$$\text{Re} = \frac{VD_o}{\nu} \tag{1}$$

$$\text{Ro} = \frac{\Omega D_o}{V} \tag{2}$$

$$\text{Gr} = \frac{g\beta\Delta TL^3}{\nu^2} \tag{3}$$

$$Nu = hD_o / k_{oil} = \frac{(Q_{in} - Q_{loss})D_o}{A(T_w - T_b)k_{oil}} \tag{4}$$

The method of estimating the heat loss is to close the outlet of the pipeline of the test section so that no outer fluid would get in the channel. Then, heat the test section with electric current. Since there is no outside air flow and heat exchange with those in the pipe, it is pure natural convection in the pipeline. The energy balance equation can be expresses as followed:

$$Q_{in} = V \times I \tag{5}$$

$$Q_{in} = Q_{loss} + hA(T_w - T_b) \tag{6}$$

Without air flowed into the test section and the wall temperature already remained stable, the natural convection $hA(T_w - T_b)$ equals to zero because the temperature of the air of natural flow is the same as the wall temperature. After the heat input from the film heater will be borne by the external environment and the test section for heat exchange. The equation can be expresses as followed:

$$Q_{in} = Q_{loss} = C_n(T_w - T_b) \text{ (the value of n is between 1~19)} \tag{7}$$

When we estimated the heat loss, we entered 0.15W~7.75W into the test section and we recorded the wall temperature and the temperature of the external environment when the temperature of the test section reached stable under different heating. We took the advantage of the relationship of the temperature difference between wall temperature and the temperature of the external environment to find the equation of estimating the heat loss. According to the equation of estimating the heat loss, the result of every temperature measuring point is a straight line passing the origin. The method used is Root Mean Square Method and all possible errors are within 7%.

2.3. Uncertainity Analysis

The errors in the temperature reading were obtained by calibrating the thermocouples. The uncertainty was $\pm 0.1°C$ from

the readout of data recorder. The difference between wall temperature and bulk temperature is greater than 62°C. The rotational speed was detected by a tachometer with a bit of oscillation. Notably, the maximum error of the rotational speed was 2% at 2500rpm. The analysis included uncertainties of oil thermophysical properties. Uncertainties in parameters were estimated by using the root-sum-square method of Kline and McClintock [8]. The measured value and its uncertainty can be expressed as $R = R \pm \delta R$. The uncertainties of Re, Ro, Re_Ω, Gr, Gr_Ω, and Nu were estimated within $\pm 2.5\%$, $\pm 2.2\%$, $\pm 2.6\%$, $\pm 5.1\%$, $\pm 5.4\%$ and $\pm 6.23\%$, respectively.

2.4. Mathematical Equations and Numerical Procedure

In order to simplify the present problem, some assumptions were made as follows: (1) the fluid flow is in the steady state, laminar and incompressible; (2) the properties of the fluid are constant, and (3) the flow field is axial symmetric (i.e. $\partial/\partial\theta=0$). The following dimensionless groups are introduced to facilitate the dimensionless transformation of these equations.

$$R = \frac{r}{\delta}, \ Z = \frac{z}{\delta}, \ U_r = \frac{u_r}{r_i\Omega}, \ U_\theta = \frac{u_\theta}{r_i\Omega}, \ U_z = \frac{u_z}{r_i\Omega}, \ \text{Re} = \frac{r_i\Omega\delta}{\nu}, \ \text{Pr} = \frac{\nu}{\alpha}, \ \Theta = \frac{T-T_o}{T_i-T_o} \tag{8}$$

Besides, the stream function (Ψ) and vorticity (ω) are introduced.

$$U_r = -\frac{1}{R}\frac{\partial\Psi}{\partial Z}, \ U_z = \frac{1}{R}\frac{\partial\Psi}{\partial R}, \ \omega = -\frac{\partial U_z}{\partial R} + \frac{\partial U_r}{\partial Z} \tag{9}$$

Then the dimensionless governing equations can be obtained as follows.

$$-\omega = \frac{\partial^2\Psi}{\partial R^2} + \frac{\partial^2\Psi}{\partial Z^2} \tag{10}$$

$$\frac{\partial(U_r\omega)}{\partial R} + \frac{\partial(U_z\omega)}{\partial Z} - \frac{2U_\theta}{R}\frac{\partial U_\theta}{\partial Z} = \frac{1}{\text{Re}}\{\frac{\partial}{\partial R}[\frac{1}{R}\frac{\partial}{\partial R}(R\omega)] + \frac{\partial^2\omega}{\partial Z^2}\} \tag{11}$$

$$U_r\frac{\partial U_\theta}{\partial R} + U_z\frac{\partial U_\theta}{\partial Z} + \frac{U_r U_\theta}{R} = \frac{1}{\text{Re}}[\frac{1}{R}\frac{\partial}{\partial R}(R\frac{\partial U_\theta}{\partial R}) + \frac{\partial^2 U_\theta}{\partial Z^2} - \frac{U_\theta}{R^2}] \tag{12}$$

$$U_r(\frac{\partial\Theta}{\partial R} + U_z\frac{\partial\Theta}{\partial Z}) = \frac{1}{\text{Re}\,\text{Pr}}[\frac{1}{R}\frac{\partial}{\partial R}(R\frac{\partial\Theta}{\partial R}) + \frac{\partial^2\Theta}{\partial Z^2}] \tag{13}$$

Boundary conditions [9] are as follows.

$$U_\theta = \Psi = \frac{\partial\Theta}{\partial Z}0, \ \omega = \frac{-1}{R}\frac{\partial^2\Psi}{\partial Z^2} \qquad at\ Z=0\ and\ Z=L/r_i \tag{14}$$

$$U_\theta = \Theta = 1, \ \Psi = 0, \ \omega = \frac{-\partial}{\partial R}\left(\frac{1}{R}\frac{\partial\Psi}{\partial R}\right) \qquad at\ R=r_i/\delta \tag{15}$$

$$U_\theta = \Psi = \Theta = 0, \ \omega = \frac{-\partial}{\partial R}\left(\frac{1}{R}\frac{\partial\Psi}{\partial R}\right) \qquad at\ R=r_o/\delta \tag{16}$$

The governing equations were discretized according to the power-law scheme proposed by Patankar [10]. All discretized algebraic equations were solved by using the SIS (Strong Implicit Solver) algorithm developed by Lee [11]. The velocity components U_r and U_z were determined from the stream function. When the velocity components had been determined, the energy equation was solved to yield the temperature distribution. The solutions were verified by varying the grid spacing and the convergence criterion. A high density grid node was used near the walls to predict the flow fields accurately. The number of grid-cells in the flow direction was 1001, and that perpendicular to the flow was 61. The convergence criterion is $Max\left|\left(F^{(n)} - F^{(n-1)}\right)/\left(F_{max}^{(n)} - F_{min}^{(n)}\right)\right| \leq 1\times10^{-5}$ where F is Ψ, ω, U or Θ.

3. Results and Discussion

Fig. 3 shows the relationships of the test modules and the wall temperatures at $q_{in} = 0.18 W/cm^2$. The result illustrated that when the rotating axis stops, that is when $Ro = 0$, both ends of the wall temperature showed a downward trend because the effect of import and export. The two ends of the outlets of the pipeline are the closest to the external environment, so they are most affected by the external environment and heat will be dissipated to both sides of the pipeline, leading lower temperature at both ends.
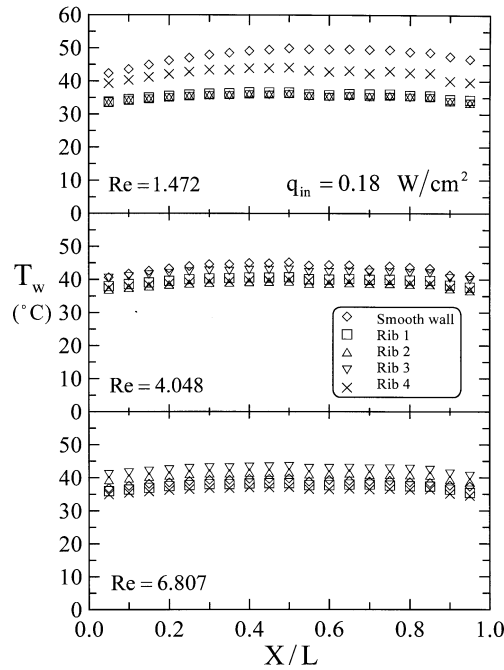
Fig. 3 Local temperature distributions for various test sections at different Reynolds numbers

Fig. 4 shows the heat transfer efficiency when $q = 0.18 \ W/cm^2$ and Re=6.807 and Ro=43.705. Generally speaking, the heat convection in Rib 4 is the best. In addition, the outlet has upwards trend caused by the export effect at the rotating condition.
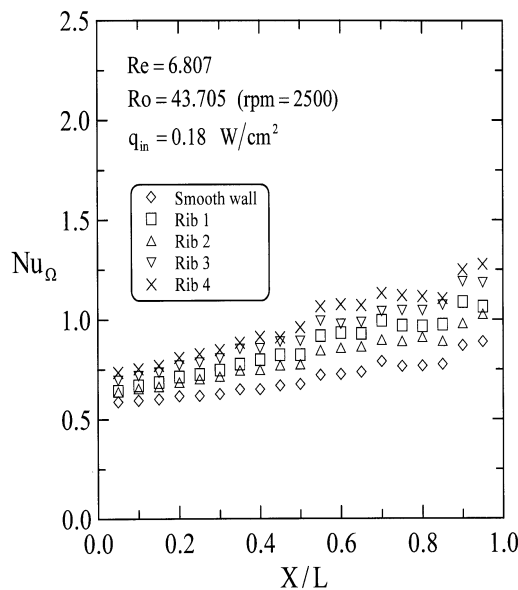

Fig. 4 Local *Nu* distributions for various test sections at Re = 6.807 and Ro = 43.705

When the forced convective parameter Re=1.472, 4.048 and 6.807, we compared the heat transfer efficiency of rotating axis between five test modules as shown in Fig. 5. The general performance of Rib 4 is the best. When the rotation number increases, the heat transfer efficiency increases. Usually the higher the heat convection passes through, the better the buoyancy is. It means that when the machining tool's axis rotates in high speed and generates high temperature and high buoyancy of the tribological oil will increase the heat convection efficiency. Fig. 6 indicates that the higher rotation number resulted in a higher heat transfer enhancement by comparing with those at stationary condition, especially for Rib 4.
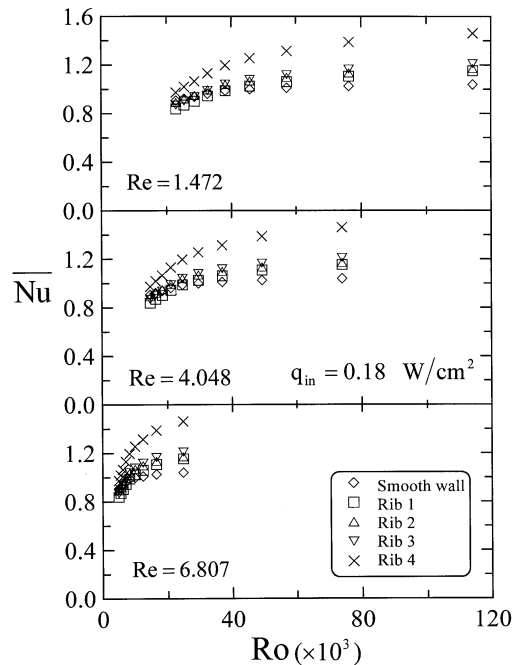

Fig. 5 Average Nusselt number as a function of Rotation number
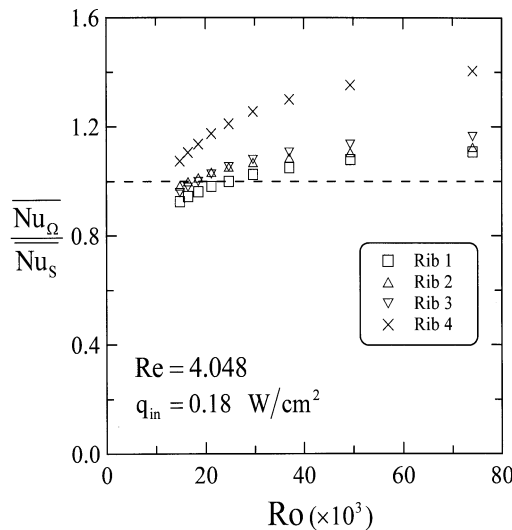
Fig. 6 Heat transfer enhancement of rotation for various Ro at $Re = 4.048$ and $q_{in} = 0.18 \ W/cm^2$

Finally, Figs. 7 to Fig. 9 shows $Nu/\sqrt{Re}$ as a function of Gr/Re^2 for various Re and q_{in}. The empirical formula of Nu in terms of Re and Gr, based on the test results, was proposed in Table 1.

Table 1 The empirical formula of *Nu* in terms of *Re* and *Gr*

Re	$Nu/\sqrt{Re} = C_1\left(Gr/Re^2\right)^{C_2}$								
	q= 0.45W/cm2			*q*= 0.18W/cm2			*q*= 0.4175W/cm2		
	C_1	C_2	*rms*(%)	C_1	C_2	*rms*(%)	C_1	C_2	*rms*(%)
1.472	162.666	-17.38	0.248	1.90E+050	-12.27	0.012	1.47E+037	-8.99	0.001
4.048	1.61E+053	-16.78	0.033	1.58E+042	-13.17	0.007	1.56E+035	-10.89	0.002
6.807	7.98E+045	-16.92	0.027	5.44E+035	-13.03	0.005	2.56E+029	-10.61	0.001
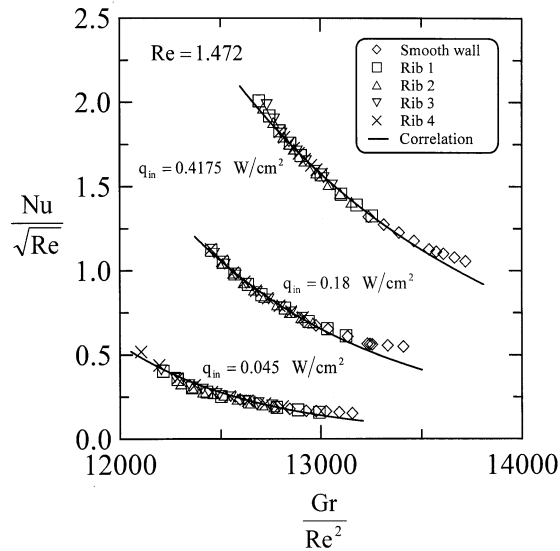
Fig. 7 $Nu/\sqrt{Re}$ as a function of Gr/Re^2 for various q_{in} at Re=1.472
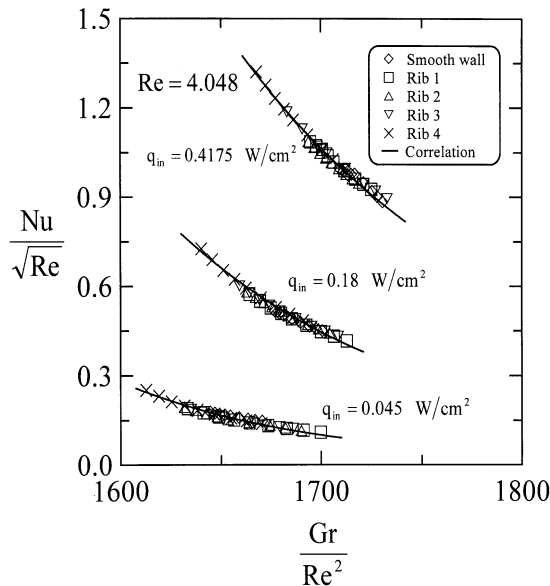

Fig. 8 $Nu/\sqrt{Re}$ as a function of Gr/Re^2 for various q_{in} at Re= 4.048
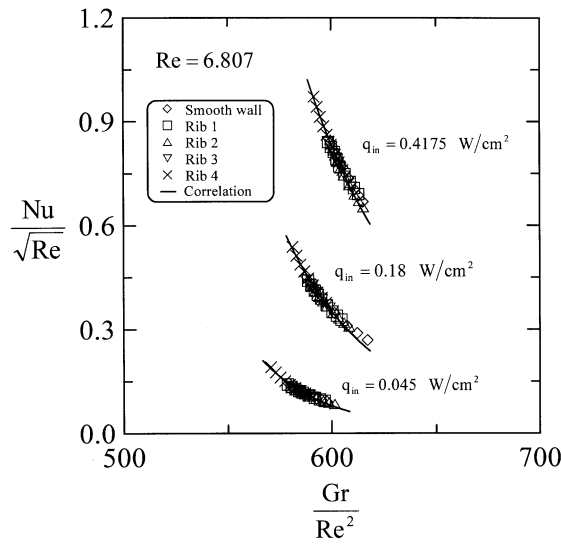
Fig. 9 $Nu/\sqrt{Re}$ as a function of Gr/Re^2 for various q_{in} at Re=6.807
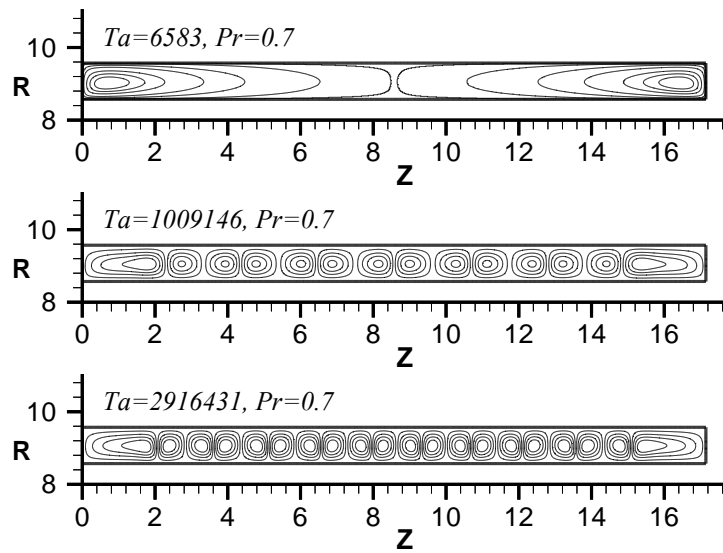

Fig. 10 Streamlines for Taylor-Couette Flow in Mode A (with smooth wall)
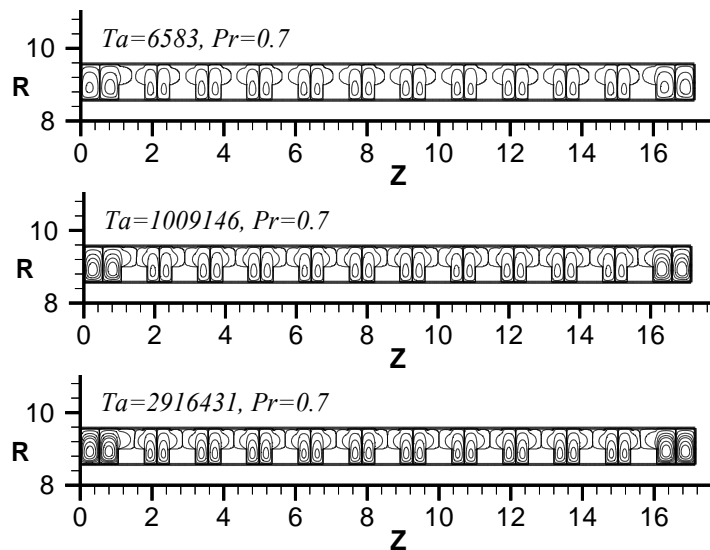
Fig. 11 Streamlines for Taylor-Couette Flow in Mode B (with ribbed wall)
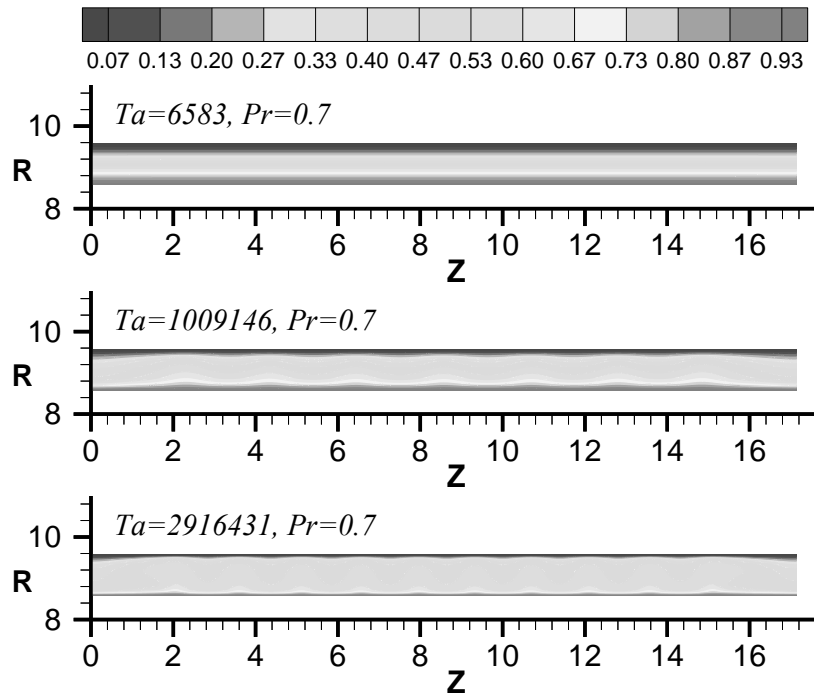
Fig. 12 Isothermal Lines for Taylor-Couette Flow in Mode A (with smooth wall)
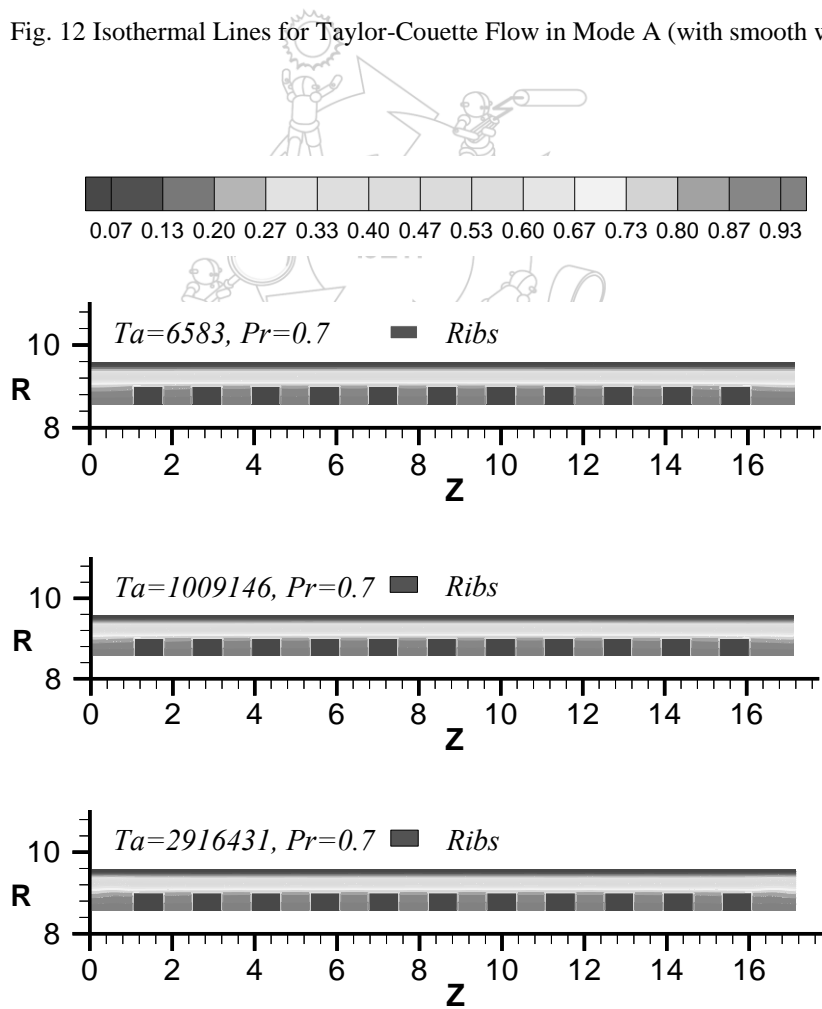
Fig. 13 Isothermal Lines for Taylor-Couette Flow in Mode B (with ribbed wall)

Fig. 10 shows the streamlines in Mode A (with smooth wall). The results depicts that the vortices began to occur at the two end sides of the annular channel as Ta=6583. When Taylor number equals 1009146, 7 pairs of vortices clearly appeared. The vortices became 10 pairs as Taylor number increased to be 2916431. The present numerical model seems to successfully predict Taylor vortices. However, the assumption of steady-state flow might reduce some flow perturbations, resulting in an over-predicted critical Taylor number (Theoretical critical Ta=1708). Fig. 11 displays the streamlines in Mode B (with ribbed wall). As shown, a complete pair of vortex could be found between adjacent ribs, but the vortices did not obviously occur at the space over the ribs. It may be also attributed to the assumption of steady-state flow. Fig. 12 and 13 depict the isothermal lines in Mode A (with smooth wall) and in Mode B (with ribbed wall), respectively. As shown in Mode A (with smooth wall), the temperature gradient near wall became sharp when Taylor number increased. However, in Mode B (with ribbed wall), the contours of temperature had little change with various Taylor numbers. It might be because of effective Taylor number and needed further study.

4.   Conclusions

According to the tests above, the conclusions can be drawn as the followings:

(1) When the rotating axis stay still, both ends of the wall temperature showed a downward trend.

(2) At rotating condition, the heat convection in Rib 4 is the best. In addition, the outlet has upwards trend caused by the export effect at the rotating condition.

(3) The higher rotation number resulted in a higher heat transfer enhancement by comparing with those at stationary condition, especially for Rib 4.

 (4) The empirical formula of *Nu* in terms of *Re* and *Gr*, based on the test results, was proposed .

Acknowledgements

References

[1]   Song F., Ewing D. and Ching C. Y., "Experimental investigation on the heat transfer characteristics of axial rotating heat pipes," Int. J. Heat Mass Transfer, vol. 47, pp.4721-4731, 2004.

[2]   Bouafia, M., Bertin, Y., Saulnier, J. B. and Ropert, P., "Experimental analysis of heat transfer in a narrow and grooved annular gap with rotating inner cylinder," Int. J. Heat Mass Transfer, vol. 41, pp. 1279-1291, 1998.

[3]   Hwang, J. J. and Lai, D. Y., "Three-dimensional mixed convection in a rotating multiple-pass square channel," Int. J. Heat Mass Transfer, vol. 41, pp. 979-991, 1998.

[4]   Kolyshkin, A. A. and Vaillancourt, Rémi., "Linear stability of Couette flow with rotating inner cylinder and radially nonuniform internal heat sources," Int. J. Heat Mass Transfer, vol. 39, pp. 537-545, 1998.

[5]   Yan, W. M. and Soong, C. Y., "Simultaneously developing mixed convection in radially rotating rectangular ducts," Int. J. Heat Mass Transfer, vol. 38, pp. 665-677, 1995.

[6]   Soong, C. Y. and Yan, W. M., "Development of secondary flow and convective heat transfer in isothermal/iso-flux rectangular ducts rotating about a parallel axis, Int. J. Heat Mass Transfer, vol. 42 pp. 497-510, 1999.

[7]   Soong, C. Y., Wu, C. C., Liu, T. P. and Liu, T. P., "Flow structure between two co-axial disks rotating independently," Experimental Thermal and Fluid Science, vol. 27, pp. 295-311, 2003.

[8]   Kline, S. J. and MaClintock, F. A., "Describing uncertainties in single sample experiments," Mechanical Engine*ering*, pp. 3-8, 1953.